INORGANIC CHEMISTRY FRONTIERS

RESEARCH ARTICLE

View Article Online
View Journal | View Issue

Cite this: *Inorg. Chem. Front.*, 2023, **10**, 1919

Dramatically improved optical anisotropy by realizing stereochemically active lone pairs in a sulfate system, $K_2SO_4{\cdot}HIO_3$†

Zhiyong Bai and Kang Min Ok *

Received 31st January 2023,
Accepted 20th February 2023

DOI: 10.1039/d3qi00192j

rsc.li/frontiers-inorganic

Obtaining sulfate-based materials with large birefringence is of great challenge due to the weak polarizability anisotropy of the constituting spherical SO_4^{2-} tetrahedron. Here, we have implemented a polyhedron of stereoactive lone pair cations, IO_3^- to the system to tackle the issue. Centimetre-sized single crystals of an alkali metal sulfate iodate, $K_2SO_4{\cdot}HIO_3$, have been readily grown by an accessible solution–evaporation method. Optical measurements on $K_2SO_4{\cdot}HIO_3$ single crystals reveal that the reported material exhibits a 70-fold increase in birefringence (*ca.* 0.14 at 589.3 nm) compared to that of the singular sulfate, K_2SO_4. In addition, $K_2SO_4{\cdot}HIO_3$ exhibits a blue-shifted UV cutoff edge of 275 nm, 25 nm shorter than that of α-HIO_3, highlighting the key role of the SO_4^{2-} tetrahedron in broadening the transmittance window.

Introduction

Birefringence (Δn) refers to an optical property of an optically anisotropic material with a refractive index that varies with the polarization and direction of propagation of light. As an important optical functionality, birefringence is of great significance for specific optical materials. For instance, a sufficient Δn is inevitably required for nonlinear optical crystals to achieve a necessary phase matching condition.[1–4] In addition, birefringent materials can be used to effectively isolate light through modulation such as polarization, and are widely used in various scientific and industrial fields such as advanced scientific instruments, laser industry, optical communication, and polarimetry.[5–11] Commonly applied birefringent materials, including calcite, YVO_4, TiO_2, β-BaB_2O_4, and MgF_2 remain inherently deficient. For example, β-BaB_2O_4 suffers from phase transition problems during crystal growth processes, while MgF_2 has small birefringence. Therefore, developing new birefringent materials is becoming a research hotspot.[12–16]

For NLO crystals, it is generally believed that too much birefringence creates a walk-off effect, which often results in lower conversion efficiency. However, the double refraction represents a more powerful and efficient device; therefore, the stronger the better when it comes to birefringent materials. From the viewpoint of the structure–property relationship, birefringence is strongly correlated with the anisotropy of polarizability of structural units. Anionic moieties with π-conjugated planar configurations such as BO_3^{3-}, CO_3^{2-}, NO_3^-, $B_3O_6^{3-}$, and $H_xC_3N_3O_3^{3-x}$ usually exhibit strong polarization anisotropy due to the large distinction between in-plane and out-of-plane optical anisotropy. Thus, the groups have been widely employed to design superior birefringent materials.[17–23] Contrary to the groups mentioned above, some non-planar and/or non-π-conjugated functional groups, especially the tetrahedrally coordinated SO_4^{2-} and PO_4^{3-} units, are often used in the synthesis of optically functional materials attributable to their exceptional ability to create large band gaps. However, because the polarization anisotropy is much smaller, it is difficult to fabricate useful birefringent materials using only polyhedra with non-planar moieties.[24–29]

One well-accepted strategy is to introduce stereochemically active lone pair (SCALP) metal cations such as Sn^{2+} or Sb^{3+}, which can readily form off-centered polyhedra and induce larger birefringence. For example, by incorporating Sn^{II}–O–X polyhedra into phosphates, the Pan group discovered that the resulting materials, Sn_2PO_4X (X = Cl, Br, and I), exhibit enhanced birefringence of greater than 0.2 at 1064 nm.[30] Also, Zou and coworkers reported that Sb^{3+} containing phosphates and sulfates, *i.e.*, $K_2SbP_2O_7F$ and $CsSbSO_4F_2$, respectively, show large enhancements in birefringence.[31,32]

In addition to Sn^{2+} and Sb^{3+}, the SCALP cation, I^{5+}, which tends to form strongly distortive IO_3^- ions, may also trigger large birefringence.[33,34] More importantly, the single crystal

Department of Chemistry, Sogang University, Seoul, 04107, Republic of Korea. E-mail: kmok@sogang.ac.kr

†Electronic supplementary information (ESI) available: CIF; detailed crystallographic data, BVS, measured refractive index data, asymmetric units, TG curves, PXRD patterns, and band structures. CCDC 2237869. For ESI and crystallographic data in CIF or other electronic format see DOI: https://doi.org/10.1039/d3qi00192j

growth ability of iodates has been significantly confirmed.[35] Although several IO_3^- containing phosphates or sulfates for NLO materials have been discovered, studies on using such modules exclusively to design phosphate- or sulfate-based birefringent materials still receive less attention.[36–38] Driven by these insights, a new birefringent material, namely, $K_2SO_4{\cdot}HIO_3$, has been successfully prepared by reacting HIO_3 with potassium sulfate, which exhibits significantly improved birefringence when compared to the singular sulphate. In this work, we demonstrate elaborate investigations of single crystal growth, structural description, optical characterization, and density functional theory (DFT) calculations to elucidate the structure–property relationship.

Results and discussion

Single crystal growth

Single crystals of $K_2SO_4{\cdot}HIO_3$ can be grown by slowly evaporating the aqueous solution containing stoichiometric amounts of K_2SO_4 and HIO_3. During the initial growth period, another plate-shaped phase, $KH(IO_3)_2$, nucleated and grew rapidly. After that, this phase gradually dissolved and disappeared, and the target material, $K_2SO_4{\cdot}HIO_3$, began to appear and grew into large single crystals. The powder X-ray diffraction (PXRD) pattern of ground crystals indicates that the main product is $K_2SO_4{\cdot}HIO_3$ together with a small amount of $KH(IO_3)_2$. This phenomenon implies that crystals of $KH(IO_3)_2$ and $K_2SO_4{\cdot}KHIO_3$ grow competitively in the solution. To suppress the growth of the by-product, the initially formed $KH(IO_3)_2$ crystals were filtered. When the filtrate is evaporated after filtering twice, only single crystals of $K_2SO_4{\cdot}HIO_3$ are formed and colourless centimetre-sized block-shaped single crystals can be harvested after about a month of growth (Fig. 1a). The PXRD pattern of the ground bulk crystals of $K_2SO_4{\cdot}HIO_3$ is consistent with the simulated one, indicating a pure phase (Fig. 1b).

Crystal structure

The title compound crystallizes in the centrosymmetric space group, $P2_1/m$ (no. 11) belonging to the monoclinic crystal system (Table S1†). The asymmetric unit consists of two independent K, one I, one S, one H, and seven O atoms (Fig. S1†). As depicted in Fig. 2a, the S atom is connected to O2, O3, O4, and O5 to form a SO_4 tetrahedron with the S–O distances varying from 1.4610(15) to 1.4928(15) Å, and the I atom is linked to O1, O6, and O7 atoms to generate an IO_3 pyramidal group with the I–O lengths varying from 1.7841(14) to 1.9132 (15) Å. Obviously, the lengths of both S–O and I–O bonds are in the normal range. The K atom is bonded to four IO_3 pyramids by sharing corners and to three SO_4 groups by sharing two corners and one edge. Disordered hydrogen atoms occupy two sites in H3 and H6 with an occupancy of 0.25 and 0.75, respectively. The H3 atom is linked to the O3 atom of the SO_4 group and the H6 atom is connected to the O6 atom of the IO_3 unit. Hydrogen bonds were calculated using the PLATON program and the results are shown in Table S6† and Fig. 2b. For the H3 atom, the acceptor is the O7 atom with an H···A distance of 2.19(8) Å, and the acceptor of the H6 atom is assigned to the O2 atom with a shorter H···A length of 1.68(18) Å. Hydrogen bonds hold the SO_4 and IO_3 groups together and are further linked by the $K1O_8$ and $K2O_8$ polyhedra to create a three-dimensional structure. The IO_3^- and SO_4^{2-} groups alternate in a well-ordered $-IO_3^-–IO_3^-–SO_4^{2-}–SO_4^{2-}-$ arrangement (Fig. 2c).

The bond valence sum (BVS) values for I, S, and K atoms are calculated to be +4.843, +5.995, and +1.13–+1.175, respectively, which are in good agreement with their normal oxidation states. While the BVS values of O1, O3, O4, O5, and O7 are in the normal range (−1.867 to −2.196), those for O2 and O6 are unusually small (−1.795 and −1.548), indicating their connections with hydrogen atoms as evidenced by single crystal XRD.

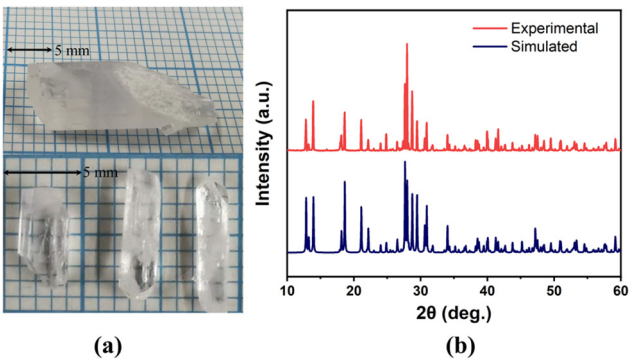

Fig. 1 (a) Photographs of as-grown single crystals and (b) powder XRD patterns of ground crystals for $K_2SO_4{\cdot}KHIO_3$.

Ultraviolet–visible (UV-vis) transmittance spectrum

The UV-Vis transmittance spectrum was obtained using a single crystal oriented in the *c*-direction. As shown in Fig. 3, the UV cut-off edge of the title compound is 275 nm, corresponding to $E_g \approx 4.50$ eV. It is noteworthy that the cut-off edge of our compound is 25 nm shorter than that of α-HIO_3, highlighting the key role of the SO_4 group in transparency in the structure. The band gap of $K_2SO_4{\cdot}HIO_3$ is comparable to those of compounds with lone pair cations such as $[Al(H_2O)_6](IO_3)_2(NO_3)$, $M(IO_3)_2(NO_3)$ (M = In and Sc), and $SnHPO_3F$.[39–42] Thus, the title compound could be applied in the UV region.

Thermogravimetric analysis (TGA)

To examine the thermal stability of $K_2SO_4{\cdot}HIO_3$, TGA was performed. As displayed in Fig. S2,† there are two stages of weight loss. Initially, the title compound thermally decomposes at about 203 °C. The experimental weight loss of *ca.* 3.03% is consistent with the calculated value (2.57%) assuming a release of 0.5 H_2O. In the second stage, starting at *ca.* 364 °C, the total experimental weight loss is about 50.03%, assuming a final residue of K_2SO_4 (cal. 48.94%). The thermal decomposition product is identified by PXRD measured after heating the title compound at 700 °C in air (Fig. S3†).

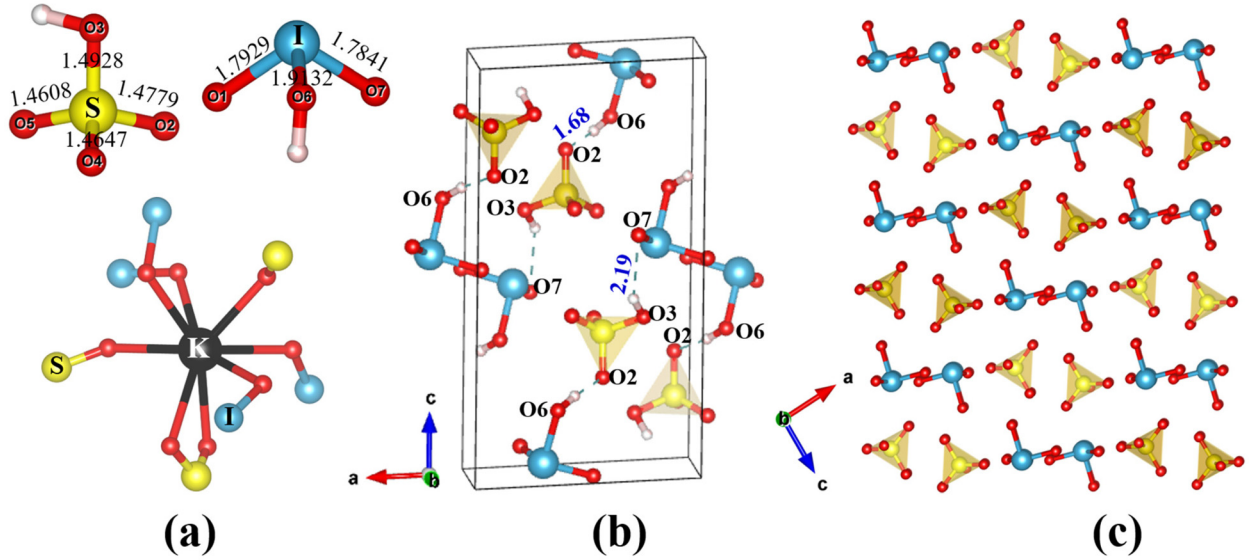

Fig. 2 The crystal structure of $K_2SO_4{\cdot}HIO_3$. (a) Coordination environment of S, I, and K atoms. (b) Hydrogen bonding interactions observed from $IO_2(OH)$ and $SO_3(OH)$ polyhedra. (c) The well-ordered arrangement of IO_3^- and SO_4^{2-} groups in the structure.

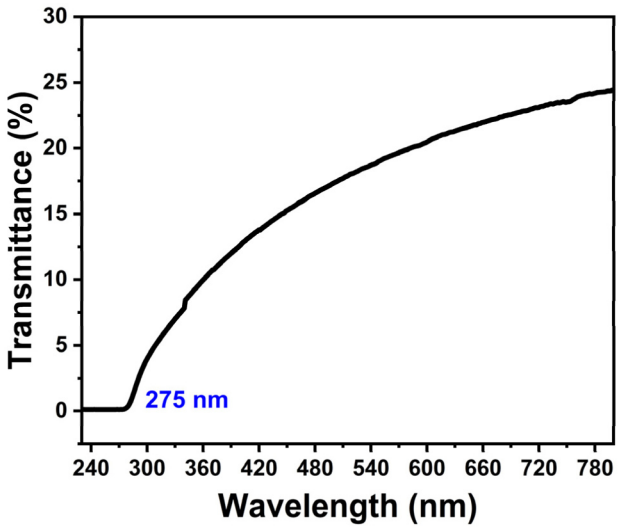

Fig. 3 The UV-vis transmittance spectrum measured on a single crystal oriented in the *c*-direction.

Birefringence

Since $K_2SO_4{\cdot}HIO_3$ belongs to the monoclinic crystal system (point group: 2/*m*), the material belongs to the biaxial crystal system according to linear optical classification; thus, it has three unequal principal refractive indices, *i.e.*, $n_x \neq n_y \neq n_z$. In this case, a (001) oriented single crystal with a size of 4.0 × 2.5 × 1.0 mm^3 exhibiting strong (00*l*) diffractions was used for birefringence measurements by employing an oil immersion technique (Fig. 4a and Table S10†). As seen in Fig. 4b, the maximum and minimum *n* values are measured as 1.675 and 1.535, respectively. Based on the properties of the refractive index ellipsoid (Fig. 4c), the birefringence of the title compound is determined to be ≥0.14 at 589.3 nm. It should be noticed that the experimental birefringence has about a 70-fold improvement for the reported material compared to K_2SO_4 (Fig. 4d).

It is noteworthy that monovalent metal sulphates have several interesting examples presented to enhance birefringence. The first example is ASO_3F (A = alkali metal cations and NH_4^+), where the authors attempted to generate a heteroanion, $(SO_3F)^-$ structural module, by chemically substituting one oxygen atom in the homoanion $(SO_4)^{2-}$ group with fluorine (Fig. 4e and f).[43] DFT calculations indicate that $(SO_3F)^-$ possesses a greater polarization anisotropy than $(SO_4)^{2-}$; thus, ASO_3F reveals larger birefringence than A_2SO_4. For the potassium member, for example, the birefringence is enhanced about 10 times from K_2SO_4 to KSO_3F.

Another example is the $[Ag(NH_3)_2]_2SO_4$ crystal, which has a sharp increase in birefringence compared to the corresponding Ag_2SO_4 (cal. 0.102 *vs.* 0.012 at 1064 nm).[44] The unique linear rod structure of $[Ag(NH_3)_2]^+$ with overwhelming polarization anisotropy is thought to be the main cause of the improved birefringence (Fig. 4g). It should be emphasized that $K_2SO_4{\cdot}HIO_3$, designed by a lone pair-directed strategy, exhibits exceptionally enhanced birefringence. This suggests that our strategy of improving optical anisotropy and enhancing birefringence by introducing IO_3^- groups into the sulphate is highly effective.

DFT calculations

To elucidate the origin of the optical properties of $K_2SO_4{\cdot}HIO_3$, the band structure, refractive index, and density of states (DOS) based on the DFT theory were determined. As presented in Fig. S5,† the band gap inferred from the band structure is 4.10 eV, which is very close to the experimental value (4.50 eV).

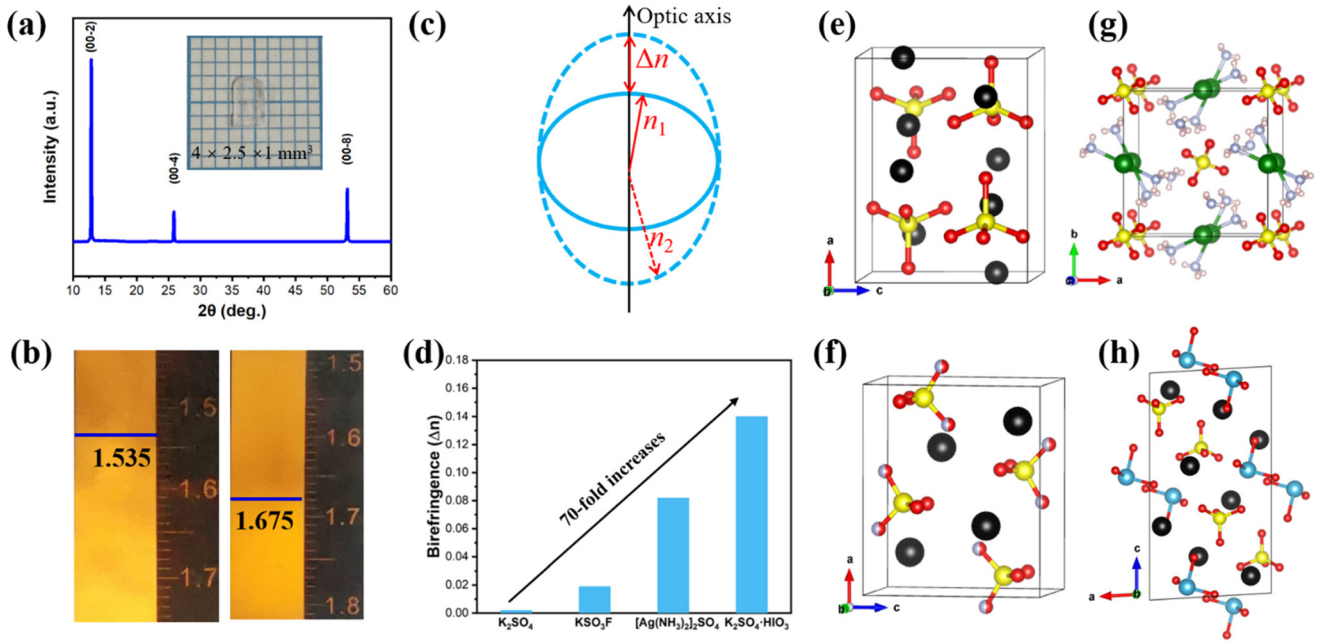

Fig. 4 (a) PXRD pattern of a (001)-oriented single crystal slice used for refractive index measurements using the oil immersion method. (b) The smallest and largest refractive indices measured. (c) Two-dimensional projection of the refractive index ellipsoid of a biaxial crystal. Δn equals the difference between the smallest n_1 and the largest n_2. (d) Birefringence plots of K_2SO_4, KSO_3F, $[Ag(NH_3)_2]_2SO_4$, and $K_2SO_4{\cdot}HIO_3$. Crystal structures of (e) K_2SO_4, (f) KSO_3F, (g) $[Ag(NH_3)_2]_2SO_4$, and (h) $K_2SO_4{\cdot}HIO_3$ (black: K, yellow: S, navy blue: I, green: Ag, red: O, silver: F, pale silver: N, and pale pink: H).

From the refractive index dispersion curves (Fig. S6†), the birefringence is determined to be 0.11 at 586 and 593 nm, which is close to the experimental value (0.14 at 589.3 nm). As can be seen in the DOS, the conduction band maximum (CBM) is dominated by the O-2p, I-5p, and I-4d states, while the valence band minimum (VBM) is mainly composed of O-2p, O-2s, I-5p, and S-3p (Fig. 5). Since the optical properties of the compounds are closely related to the behaviour of electrons in the VBM and CBM, it can be concluded that the optical properties of $K_2SO_4{\cdot}HIO_3$ are synergistically determined by the IO_3^- and SO_4^{2-} groups. Moreover, because the small birefringence of the monosulfate, K_2SO_4, is attributed to the weakly anisotropic SO_4^{2-} tetrahedron, the greatly enhanced birefringence in $K_2SO_4{\cdot}HIO_3$ should have originated from the IO_3^- group.

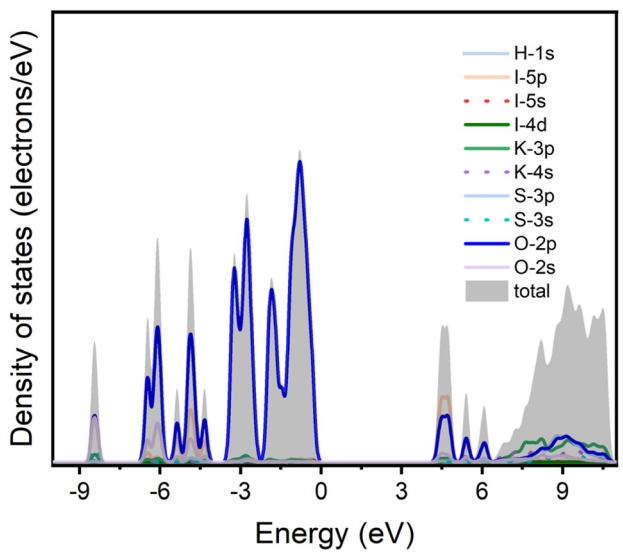

Fig. 5 The total and partial DOS of $K_2SO_4{\cdot}HIO_3$.

Conclusions

In summary, a new birefringent material, $K_2SO_4{\cdot}HIO_3$, containing two types of anionic groups has been discovered. In particular, the birefringence of $K_2SO_4{\cdot}HIO_3$ is greater than that of previously developed KSO_3F and $[Ag(NH_3)_2]_2SO_4$, and is 70 times higher than that of K_2SO_4 attributable to the successful combination of IO_3^- units. The finding indicates that sulfates can be a class of very effective systems for improving the optical anisotropy once polyhedra of lone pair cations are successfully introduced. There is no doubt that such a methodology can also be applied to other systems with poor-birefringence, such as phosphates and silicates, to fabricate functional materials with enhanced optical anisotropy.

Experimental

Crystal growth

Potassium sulfate (K_2SO_4, S. P. C. GR Reagent, first grade) and iodic acid (HIO_3, Alfa Aesar, 99%) were used as starting

reagents. In typical experiments, stoichiometric amounts of K_2SO_4 (28.4 mmol, 4.94 g) and HIO_3 (28.4 mmol, 5.00 g) were dissolved in 100 mL of deionized water and stirred at 80 °C for 1 h to allow the solution to become clear. The clear solution was continued to heat until 50 mL of concentrated solution was obtained. After filtering twice, the flask containing the solution was sealed with a perforated plastic film and the solution was slowly evaporated at room temperature. Colorless centimeter-sized block-shaped single crystals were harvested in about one month of growth. The PXRD pattern of the ground bulk crystals agrees well with the simulated pattern.

PXRD

PXRD data were collected at room temperature on a Rigaku MiniFlex 600 diffractometer equipped with Cu Kα radiation (λ = 1.5406 Å). The 2θ range was 10–60° with a scan step width of 0.02° and a fixed counting time of 5 s per step.

Single-crystal structure determination

The single crystal X-ray diffraction data were collected on a Bruker APEX-II CCD diffractometer utilizing Mo Kα radiation (λ = 0.71073 Å) at 300(2) K at the Advanced Bio-Interface Core Research Facility at Sogang University. Data reduction, cell refinement, and absorption corrections were conducted with the program APEX 4. The structure was solved by the intrinsic phasing method and refined on F^2 by full-matrix least-squares techniques using the program Olex2.[45] The structure was checked using the program PLATON and no higher symmetry was found.[46] Crystal data and detailed structural information are given in Tables S1–S8.†

Refractive index measurements

The refractive index was measured using an oil immersion technique on a gem refractometer equipped with a sodium yellow laser (λ = 589.3 nm). The refractive index was recorded for every 45-degree rotation.

UV-vis spectroscopy

UV–vis transmittance spectra were collected on a JASCO V-660 spectrometer in the wavelength range of 200–800 nm using a (001)-oriented single crystal slice.

Infrared (IR) spectra

IR spectra were recorded on a Nicolet AVATAR 330 FT-IR spectrometer in the wavenumber range of 650 to 4000 cm^{-1}.

TGA

TGA was performed by using a SCINCO TGA-N 1000 thermal analyzer. A 6.6 mg portion of powder sample was loaded in an alumina crucible and heated from 25 to 800 °C at a rate of 10 °C min^{-1} under flowing air.

Theoretical calculations

The band structure and DOS of $K_2SO_4{\cdot}HIO_3$ were calculated by employing a QUANTUM ESPRESSO program based on the DFT. The optical properties of $K_2SO_4{\cdot}HIO_3$ were calculated using CASTEP.[47] The ultrasoft pseudopotential types with non-linear core correction,[48] Perdew–Burke–Ernzerhof exchange–correlation function,[49] and scalar relativistic effect were applied. The valence electrons of K-3p4s, I-4d5p5s, S-3p3s, O2-2p2s, and H-1s were used in the calculations. The *k*-points of the Brillouin zone were set to be 4 × 4 × 2. The other parameters were set as default.

Conflicts of interest

There are no conflicts to declare.

Acknowledgements

This work was supported by the National Research Foundation of Korea (NRF) funded by the Ministry of Science and ICT (grant no. 2018R1A5A1025208 and 2019R1A2C3005530).

References

1 M. Mutailipu, K. R. Poeppelmeier and S. Pan, Borates: a rich source for optical materials, *Chem. Rev.*, 2021, **121**, 1130–1202.
2 M. Mutailipu, Z. Yang and S. Pan, Toward the enhancement of critical performance for deep-ultraviolet frequency-doubling crystals utilizing covalent tetrahedra, *Acc. Mater. Res.*, 2021, **2**, 282–291.
3 A. Sekar, U. R. Muthurakku and K. Sivaperuman, An overview on recent trends in deep–ultraviolet (DUV) and ultraviolet (UV) nonlinear optical crystals, *ChemistrySelect*, 2021, **6**, 10688–10716.
4 F. Yang, L. Wang, L. Huang and G. Zou, The study of structure evolvement of $KTiOPO_4$ family and their nonlinear optical properties, *Coord. Chem. Rev.*, 2020, **423**, 213491.
5 A. Tudi, S. Han, Z. Yang and S. Pan, Potential optical functional crystals with large birefringence: recent advances and future prospects, *Coord. Chem. Rev.*, 2022, **459**, 214380.
6 M. Zhang, D. An, C. Hu, X. Chen, Z. Yang and S. Pan, Rational design via synergistic combination leads to an outstanding deep-ultraviolet birefringent $Li_2Na_2B_2O_5$ material with an unvalued B_2O_5 functional gene, *J. Am. Chem. Soc.*, 2019, **141**, 3258–3264.
7 T. Tong, W. Zhang, Z. Yang and S. Pan, Series of crystals with giant optical anisotropy: a targeted strategic research, *Angew. Chem., Int. Ed.*, 2021, **60**, 1332–1338.
8 S. Niu, G. Joe, H. Zhao, Y. Zhou, T. Orvis, H. Huyan, J. Salman, K. Mahalingam, B. Urwin, J. Wu, Y. Liu, T. E. Tiwald, S. B. Cronin, B. M. Howe, M. Mecklenburg, R. Haiges, D. J. Singh, H. Wang, M. A. Kats and J. Ravichandran, Giant optical anisotropy in a quasi-one-dimensional crystal, *Nat. Photonics*, 2018, **12**, 392–396.
9 C. Jin, X. Shi, H. Zeng, S. Han, Z. Chen, Z. Yang, M. Mutailipu and S. Pan, Hydroxyfluorooxoborate $Na[B_3O_3F_2(OH)_2][B(OH)_3]$: optimizing the optical anisotropy

with heteroanionic units for deep ultraviolet birefringent crystals, *Angew. Chem., Int. Ed.*, 2021, **60**, 20469–20475.
10 Y. Li, X. Zhang, Y. Zhou, W. Huang, Y. Song, H. Wang, M. Li, M. Hong, J. Luo and S. Zhao, An optically anisotropic crystal with large birefringence arising from cooperative π orbitals, *Angew. Chem., Int. Ed.*, 2022, **61**, e202208811.
11 W. Huang, X. Zhang, Y. Li, Y. Zhou, X. Chen, X. Li, F. Wu, M. Hong, J. Luo and S. Zhao, A hybrid halide perovskite birefringent crystal, *Angew. Chem.*, 2022, **134**, e202202746.
12 G. Ghosh, Dispersion-equation coefficients for the refractive index and birefringence of calcite and quartz crystals, *Opt. Commun.*, 1999, **163**, 95–102.
13 H. T. Luo, T. Tkaczyk, E. L. Dereniak, K. Oka and R. Sampson, High birefringence of the yttrium vanadate crystal in the middle wavelength infrared, *Opt. Lett.*, 2006, **31**, 616–618.
14 J. R. DeVore, Refractive indices of rutile and sphalerite, *J. Opt. Soc. Am.*, 1951, **41**, 416–419.
15 Z. Guoqing, X. Jun, C. Xingda, Z. Heyu, W. Siting, X. Ke and G. Fuxi, Growth and spectrum of a novel birefringent α-BaB_2O_4 crystal, *J. Cryst. Growth*, 1998, **191**, 517–519.
16 M. J. Dodge, Refractive properties of magnesium fluoride, *Appl. Opt.*, 1984, **23**, 1980–1985.
17 Q. Wang, W. Song, Y. Lan, L. Cao, L. Huang, D. Gao, J. Bi and G. Zou, KLi_2CO_3F: a beryllium-free KBBF-type deep-UV carbonate with an enhanced interlayer interaction and large birefringence, *Inorg. Chem. Front.*, 2022, **9**, 3590–3597.
18 W. Xiong, L. Chen, L. Huang, F. Guo, Y. Zhou and H. Yuan, Bridgman growth and characterization of birefringent crystal $NaNO_3$, *Cryst. Res. Technol.*, 2015, **50**, 250–254.
19 Y. Long, X. Dong, L. Huang, H. Zeng, Z. Lin and G. Zou, $CsHgNO_3Cl_2$: A new nitrate UV birefringent material exhibiting an optimized layered structure, *Inorg. Chem.*, 2020, **59**, 12578–12585.
20 Z. Chen, H. Zeng, S. Han, Z. Yang and S. Pan, From $BaCl_2$ to $Ba(NO_3)Cl$: significantly enhanced birefringence derived from π-conjugated [NO_3], *New J. Chem.*, 2021, **45**, 17544–17550.
21 Z. Jia, N. Zhang, Y. Ma, L. Zhao, M. Xia and R. Li, Top-seeded solution growth and optical properties of deep-UV birefringent crystal $Ba_2Ca(B_3O_6)_2$, *Cryst. Growth Des.*, 2017, **17**, 558–562.
22 H. Zhang, M. Zhang, S. Pan, Z. Yang, Z. Wang, Q. Bian, X. Hou, H. Yu, F. Zhang, K. Wu, F. Yang, Q. Peng, Z. Xu, K. B. Chang and K. R. Poeppelmeier, $Na_3Ba_2(B_3O_6)_2F$: next generation of deep-ultraviolet birefringent materials, *Cryst. Growth Des.*, 2014, **15**, 523–529.
23 X. Hao, M. Luo, C. Lin, G. Peng, T. Yan, D. Lin, L. Cao, X. Long, G. Yang and N. Ye, $A(H_3C_3N_3O_3)(NO_3)$ (A = K, Rb): alkali-metal nitrate isocyanurates with strong optical anisotropy, *Inorg. Chem.*, 2020, **59**, 10361–10367.
24 P. Yu, L. M. Wu, L. J. Zhou and L. Chen, Deep-ultraviolet nonlinear optical crystals: $Ba_3P_3O_{10}X$ (X = Cl, Br), *J. Am. Chem. Soc.*, 2014, **136**, 480–487.
25 S. Zhao, P. Gong, S. Luo, L. Bai, Z. Lin, C. Ji, T. Chen, M. Hong and J. Luo, Deep-ultraviolet transparent phosphates $RbBa_2(PO_3)_5$ and $Rb_2Ba_3(P_2O_7)_2$ show nonlinear optical activity from condensation of $[PO4]^{3-}$ units, *J. Am. Chem. Soc.*, 2014, **136**, 8560–8563.
26 L. Li, Y. Wang, B. H. Lei, S. Han, Z. Yang, K. R. Poeppelmeier and S. Pan, A new deep-ultraviolet transparent orthophosphate $LiCs_2PO_4$ with large second harmonic generation response, *J. Am. Chem. Soc.*, 2016, **138**, 9101–9104.
27 Y. Zhou, L. Cao, C. Lin, M. Luo, T. Yan, N. Ye and W. Cheng, $AMgPO_4{\cdot}6H_2O$ (A = Rb, Cs): strong SHG responses originated from orderly PO_4 groups, *J. Mater. Chem. C*, 2016, **4**, 9219–9226.
28 Z. Bai, C. L. Hu, L. Liu, L. Zhang, Y. Huang, F. Yuan and Z. Lin, $KMg(H_2O)PO_4$: a deep-ultraviolet transparent nonlinear optical material derived from $KTiOPO_4$, *Chem. Mater.*, 2019, **31**, 9540–9545.
29 Z. Li, W. Jin, F. Zhang, Z. Yang and S. Pan, Exploring short-wavelength phase-matching nonlinear optical crystals by employing $KBe_2BO_3F_2$ as the template, *ACS Cent. Sci.*, 2022, **8**, 1557–1564.
30 J. Guo, A. Tudi, S. Han, Z. Yang and S. Pan, Sn_2PO_4I: an excellent birefringent material with giant optical anisotropy in non π-conjugated phosphate, *Angew. Chem., Int. Ed.*, 2021, **60**, 24901–24904.
31 Y. Deng, L. Huang, X. Dong, L. Wang, K. M. Ok, H. Zeng, Z. Lin and G. Zou, $K_2Sb(P_2O_7)F$: Cairo pentagonal layer with bifunctional genes reveal optical performance, *Angew. Chem., Int. Ed.*, 2020, **59**, 21151–21156.
32 X. Dong, L. Huang, C. Hu, H. Zeng, Z. Lin, X. Wang, K. M. Ok and G. Zou, $CsSbF_2SO_4$: an excellent ultraviolet nonlinear optical sulfate with a KTiOPO4 (KTP)-type structure, *Angew. Chem., Int. Ed.*, 2019, **58**, 6528–6534.
33 M. Gai, Y. Wang, T. Tong, Z. Yang and S. Pan, $ZnIO_3F$: zinc iodate fluoride with large birefringence and wide band gap, *Inorg. Chem.*, 2020, **59**, 4172–4175.
34 Y. Li and K. M. Ok, $Mg(H_2O)_6[(IO_2(OH))_2(IO_3)]_2$: a new iodate with a very large band gap and optical anisotropy, *J. Mater. Chem. C*, 2022, **10**, 8776–8782.
35 H. Wu, H. Yu, W. Zhang, J. Cantwell, K. R. Poeppelmeier, S. Pan and P. S. Halasyamani, Crystal growth and linear and nonlinear optical properties of $KIO_3{\cdot}Te(OH)_6$, *Cryst. Growth Des.*, 2017, **17**, 4405–4412.
36 H. Liu, Q. Wu, L. Liu, Z. Lin, P. S. Halasyamani, X. Chen and J. Qin, $AgBi(SO_4)(IO_3)_2$: aliovalent substitution induces structure dimensional upgrade and second harmonic generation enhancement, *Chem. Commun.*, 2021, **57**, 3712–3715.
37 H. X. Tang, Y. X. Zhang, C. Zhuo, R. B. Fu, H. Lin, Z. J. Ma and X. T. Wu, A niobium oxyiodate sulfate with a strong second-harmonic-generation response built by rational multi-component design, *Angew. Chem., Int. Ed.*, 2019, **58**, 3824–3828.
38 M. Ding, H. Yu, Z. Hu, J. Wang and Y. Wu, $Na_7(IO_3)(SO_4)_3$: the first noncentrosymmetric alkaline-metal iodate-sulfate

with isolated [IO_3] and [SO_4] units, *Chem. Commun.*, 2021, **57**, 9598–9601.

39 Z. Bai, C. L. Hu, D. Wang, L. Liu, L. Zhang, Y. Huang, F. Yuan and Z. Lin, [$Al(H_2O)_6$](IO_3)$_2$(NO_3): a material with enhanced birefringence induced by synergism of two superior functional motifs, *Chem. Commun.*, 2020, **56**, 11629–11632.

40 Y. Huang, T. K. Jiang, B. P. Yang, C. L. Hu, Z. Fang and J. G. Mao, Two indium iodate-nitrates with large birefringence induced by hybrid anionic functional groups and their favorable arrangements, *Inorg. Chem.*, 2022, **61**, 3374–3378.

41 C. Wu, X. Jiang, Z. Wang, L. Lin, Z. Lin, Z. Huang, X. Long, M. G. Humphrey and C. Zhang, Giant optical anisotropy in the UV-transparent 2D nonlinear optical material Sc(IO_3)$_2$(NO_3), *Angew. Chem., Int. Ed.*, 2021, **60**, 3464–3468.

42 H.-D. Yang, M.-Y. Ran, S.-H. Zhou, X.-T. Wu, H. Lin and Q.-L. Zhu, Rational design via dual-site aliovalent substitution leads to an outstanding IR nonlinear optical material with well-balanced comprehensive properties, *Chem. Sci.*, 2022, **13**, 10725–10733.

43 W. Jin, W. Zhang, A. Tudi, L. Wang, X. Zhou, Z. Yang and S. Pan, Fluorine-driven enhancement of birefringence in the fluorooxosulfate: a deep evaluation from a joint experimental and computational study, *Adv. Sci.*, 2021, **8**, 2003594.

44 Y. C. Yang, X. Liu, J. Lu, L. M. Wu and L. Chen, [Ag(NH_3)$_2$]$_2$$SO_4$: a strategy for the coordination of cationic moieties to design nonlinear optical materials, *Angew. Chem., Int. Ed.*, 2021, **60**, 21216–21220.

45 O. V. Dolomanov, L. J. Bourhis, R. J. Gildea, J. A. K. Howard and H. Puschmann, OLEX2: a complete structure solution, refinement and analysis program, *J. Appl. Crystallogr.*, 2009, **42**, 339–341.

46 A. L. J. Spek, Single-crystal structure validation with the program PLATON crystallography, *J. Appl. Crystallogr.*, 2003, **36**, 7–13.

47 M. D. Segall, P. J. Lindan, M. A. Probert, C. J. Pickard, P. J. Hasnip, S. J. Clark and M. C. Payne, First-principles simulation ideas, illustrations and the CASTEP code, *J. Phys.: Condens. Matter*, 2002, **14**, 2717–2744.

48 D. Vanderbilt, Soft self-consistent pseudopotentials in a generalized eigenvalue formalism, *Phys. Rev. B: Condens. Matter Mater. Phys.*, 1990, **41**, 7892–7895.

49 J. P. Perdew, K. Burke and M. Ernzerhof, Generalized gradient approximation made simple, *Phys. Rev. Lett.*, 1996, **77**, 3865–3868.